Precise *In Situ* Delivery of a Photo-Enhanceable Inflammasome-Activating Nanovaccine Activates Anticancer Immunity

Yang Zhou[1], Li Pang[2,3], Tao Ding[3], Kang Chen[1], Jinzhao Liu[1], Meicen Wu[1], Weiping Wang[1], and Kwan Man[3]

ABSTRACT

A variety of state-of-the-art nanovaccines (NV) combined with immunotherapies have recently been developed to treat malignant tumors, showing promising results. However, immunosuppression in the tumor microenvironment (TME) restrains cytotoxic T-cell infiltration and limits the efficacy of immunotherapies in solid tumors. Therefore, tactics for enhancing antigen cross-presentation and reshaping the TME need to be explored to enhance the activity of NVs. Here, we developed photo-enhanceable inflammasome-activating NVs (PIN) to achieve precise *in situ* delivery of a tumor antigen and a hydrophobic small molecule activating the nucleotide-binding oligomerization domain, leucine-rich repeat, and pyrin domain–containing protein 3 inflammasome (NLRP3) pathway. Near-infrared light irradiation promoted PIN accumulation in tumor sites through photo-triggered charge reversal of the nanocarrier. Systematic PIN administration facilitated intratumoral NLRP3 inflammasome activation and antigen cross-presentation in antigen-presenting cells upon light irradiation at tumor sites. Furthermore, PIN treatment triggered immune responses by promoting the production of proinflammatory cytokines and activating antitumor immunity without significant systematic toxicity. Importantly, the PIN enhanced the efficacy of immune checkpoint blockade and supported the establishment of long-term immune memory in mouse models of melanoma and hepatocellular carcinoma. Collectively, this study reports a safe and efficient photoresponsive system for codelivery of antigens and immune modulators into tumor tissues, with promising therapeutic potential.

Significance: The development of a photoresponsive nanovaccine with spatiotemporal controllability enables robust tumor microenvironment modulation and enhances the efficacy of immune checkpoint blockade, providing an effective immunotherapeutic strategy for cancer treatment.

See related commentary by Zhen and Chen, p. 3709

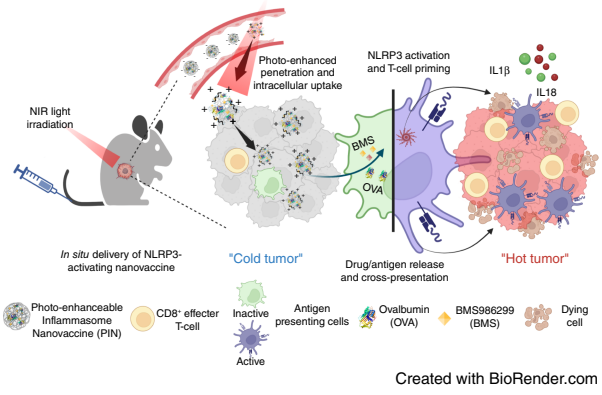

Introduction

Therapeutic advances in cancer immunotherapy have revolutionized the treatment of malignancies, such as melanoma, liver cancer, lung cancer, and leukemia (1–3). However, considerable patients with cancer treated with immunotherapy have shown poor response (4, 5). The intrinsic tumor microenvironment (TME) tends to be immunosuppressive and results in resistance to immune-stimulating therapies (6, 7). Therefore, there is an urgent need to develop new tactics to reverse the low immunogenic TME and improve the response rate of cancer immunotherapy.

Among various types of state-of-the-art immunotherapy, nanoparticle (NP)-based vaccines [nanovaccines (NV)] have received much attention due to good targeting ability to antigen-presenting cells (APC), high levels of antigen cross-presentation, and long-term immune memory against tumors (8–10). However, the majority of NVs are currently administered by either subcutaneous or intramuscular injection (9, 11), which cannot directly overcome immunosuppression in the TME. Therefore, the concept of *in situ* vaccine has been put forward, which promotes antigen production and cross-priming directly within tumors (12, 13). Although such vaccines may modulate TME with the assistance of immune-

[1]State Key Laboratory of Pharmaceutical Biotechnology, Dr. Li Dak-Sum Research Centre, Department of Pharmacology and Pharmacy, Li Ka Shing Faculty of Medicine, The University of Hong Kong, Hong Kong, China. [2]Department of Pancreato-Biliary Surgery and Liver Transplantation Center, Sun Yat-sen Memorial Hospital, Sun Yat-sen University, Guangzhou, China. [3]Department of Surgery, School of Clinical Medicine, Li Ka Shing Faculty of Medicine and HKU-SZH, State Key Laboratory of Liver Research, The University of Hong Kong, Hong Kong, China.

Y. Zhou, L. Pang, and T. Ding contributed equally to this article.

Corresponding Authors: Weiping Wang, Department of Pharmacology and Pharmacy, University of Hong Kong, Rm 56, 2/F, Lab Block, Faculty of Medicine Building, Hong Kong, 999077, China. E-mail: wangwp@hku.hk; and Kwan Man, Department of Surgery, University of Hong Kong, Rm 55, 9/F, Lab Block, Faculty of Medicine Building, Hong Kong, 999077, China. E-mail: kwanman@hku.hk.

Cancer Res 2024;84:3834–47

doi: 10.1158/0008-5472.CAN-24-0220

stimulating agents, technical difficulties and safety concerns with regard to intratumoral administration and limited intracellular translocation of tumor antigens impede their broad application for cancer immunotherapy (14, 15). Therefore, it is urgently needed to explore a novel strategy to achieve enhanced intracellular delivery of tumor antigen and immune modulators in tumor tissues with high efficiency, high specificity, and general applicability.

Inflammasomes consist of cytosolic protein elements that are assembled to mediate both the innate and adaptive immune responses (16). Inflammasome assembly promotes proteolytic cleavage of caspase-1 into cleaved caspase-1, which further initiates the production of proinflammatory IL1β and IL18 converted from dormant cytokine precursors, pro-IL1β and pro-IL18 (17, 18). It has been demonstrated that IL1β empowers dendritic cell maturation and facilitates T-cell priming (19–21), and IL18 acts as a robust enhancer in the production of IFNγ and cytotoxicity of effector T and NK cells (22–24). The activation of nucleotide-binding oligomerization domain, leucine-rich repeat, and pyrin domain–containing protein 3 (NLRP3) inflammasome pathway has been demonstrated to improve adaptive immune response against tumors (21, 25). However, undesired NLRP3 activation outside tumors might induce excessive inflammatory responses, leading to the development of inflammatory diseases, such as autoimmune diseases, inflammatory bowel disease, and rheumatoid arthritis (26–28). Therefore, it is still essential to develop a tumor-specific NLRP3 stimulation strategy to maximize therapeutic effects and avoid potential drug toxicity.

Photoresponsive nanomedicines have attracted considerable attention in recent years. Light as an external stimulus can be spatiotemporally manipulated for precise drug delivery (29–31). Recently, a photoresponsive nanocarrier self-assembled by 4,4-difluoro-4-bora-3a, 4a-diaza-s-indacene (BODIPY)–modified poly(amidoamine) (PAMAM; BMP) has been reported by our group to be a promising hydrophobic molecule and protein carrier. Herein, we hypothesized that such a dendrimer-based nanocomplex might be employed as an adjuvant carrier for the codelivery of hydrophilic antigens and hydrophobic immune modulators. This study revealed that this carrier could promote the intracellular delivery of cargo proteins and molecules simultaneously after light irradiation by charge reversal. The photo-enhanceable inflammasome-activating NVs (PIN) were fabricated by self-assembly of a model tumor antigen, ovalbumin (OVA), an NLRP3 agonist, BMS986299 (BMS), BMP, and hyaluronic acid (HA). PINs fostered a high level of antigen cross-presentation and activated the NLRP3 inflammasome pathway in APCs under near-infrared (NIR) light irradiation both *in vitro* and *in vivo*. The systematic administration of PINs could efficiently convert the "cold tumor" into the "hot tumor" upon light irradiation and enhance the therapeutic efficacy of immune checkpoint blockade (ICB) in the subcutaneous melanoma model and the orthotopic hepatocellular carcinoma (HCC) model. Moreover, long-term immune memory against rechallenged tumors was established in mouse tumor models after PIN and ICB treatment. Our work presented an effective photo-controlled strategy to induce an *in situ* adaptive immune response and long-term immune memory against tumors. The PIN system holds significant promise for future applications in the field of cancer immunotherapy.

Materials and Methods

Reagents

Compounds 2,4-dimethyl-1H-pyrrole, 2-chloro-2-oxoethyl acetate, 4-nitrophenyl chloroformatedimethyl, anhydrous DMSO (Superdry, with molecular sieves), anhydrous dichloromethane (Superdry, with molecular sieves), and anhydrous pyridine (Superdry, with molecular sieves) were purchased from J&K Chemical. Compounds N, N-diisopropylethylamine, generation 5 (G5) PAMAM, 4-anisaldehyde, and methylmagnesium bromide were ordered from Dieckmann. Chlorin e6 (Ce6) was purchased and obtained by Frontier Specialty Chemicals Inc. HA (40–100 kDa) and rhodamine B isothiocyanate were purchased from Maclin. Aspartate Aminotransferase Activity Assay Kit (MAK055) and Alanine Aminotransferase Activity Assay Kit (MAK052) were ordered from Sigma Aldrich. Opal 6-Plex Manual Detection Kit—for Whole Slide Imaging was bought from Akoya Biosciences. OVA was purchased from InvivoGen. Hoechst 33342 was obtained from Thermo Fisher Scientific. BMS986299 was purchased from MedChemExpress. Antibodies used in this study are listed in Supplementary Table S1. Primers used in this study are listed in Supplementary Table S2.

Cell lines and cell culture

B16F10 cells (murine melanoma cell line, RRID: CVCL_0159) and RAW264.7 cells (murine macrophage cell line, RRID: CVCL_0493) were obtained from the ATCC. Cell cultures were routinely tested for *Mycoplasma* infection. Short tandem repeat profiling was applied for RAW264.7 authentication. Mouse C57BL/6 syngeneic OVA-RIL-175 HCC cell line was a generous gift from Prof. Lars Zender and Prof. Stephanie Ma. The exogenous expression of OVA (257-246) and luciferase in tumor cells was achieved by lentiviral transfection. Both cell lines were cultured in complete DMEM cell culture medium containing 10% FBS, penicillin (100 μg/mL), and streptomycin (100 μg/mL) at 37°C with 5% CO_2.

Synthesis of green or NIR light-responsive BMP

The synthesis of green or NIR light-responsive BODIPY and BMP was shown in our previous study (32).

NP preparation

PINs were prepared by nanoprecipitation. Briefly, 3.2 μg BMS986299 and 16 μg OVA were added to 400 μL H_2O during vigorous stirring. NIR BMP (25 μg) was then added to the solution immediately. HA (10 μg) was then used to coat the NPs after that. After preparation, the NPs were ultracentrifuged with an ultracentrifuge tube (100 kDa, Amicon Ultra-15 Centrifugal Filter Unit) to remove unloaded small molecules and proteins. After purification, the NPs were collected and centrifuged at 4,000 rpm for 5 minutes to remove aggregates. The as-prepared NPs were then used for subsequent characterization and treatment. After lyophilization of PINs, encapsulation efficiency and loading content of BMS986299 were measured by high-performance liquid chromatography. Encapsulation efficiency and loading content of OVA were approximately quantified by calculating the value of the quantity of NPs minus the quantity of NIR light-responsive BMP (NBMP) and the quantity of BMS986299.

Zeta potential/size measurement

Zeta potential and size of PINs were measured using a Zetasizer Nano-ZS90 system. Morphology investigation was conducted using a Philips CM100 transmission electron microscope. The photoresponsiveness of PINs was determined by measuring zeta potential, size, and morphology change. Light source: LED, 660 nm, 100 mW/cm^2, 5 minutes.

Drug release measurement

The release profile of BMS from NBMP NPs was assessed using the dialysis method. NBMP NPs (500 μL) with or without light irradiation (650 nm, 100 mW/cm^2, 7 minutes) were placed in each dialysis bag (3,500 Da MWCO) and dialyzed against 7 mL of PBS buffer at 37°C. At predetermined time points (0.5, 1, 2, 4, 6, 8, 24, and 48 hours), the entire external PBS solution was replaced with fresh PBS buffer. The cumulative release percentage of BMS over time was determined by high-performance liquid chromatography analysis.

The release profile of OVA from NBMP NPs was evaluated using the ultrafiltration method. NBMP NPs (1 mL) with or without light irradiation (650 nm, 100 mW/cm^2, 7 minutes) were placed in the upper layer of the ultrafiltration tube (100 kDa MWCO) and incubated at 37°C. At predetermined time points (0.5, 1, 2, 4, 6, 8, 24, 48 hours), ultrafiltration was performed at 12,000 *g* for 1 minute. The cumulative released OVA in the lower layer over time was determined using the bicinchoninic acid assay.

Intracellular delivery efficiency

The intracellular delivery efficiency of PINs was determined by flow cytometry. Briefly, RAW264.7 cells were incubated with non-irradiated PINs and irradiated PINs for 4 hours. After light, the cells were washed with PBS and collected for fluorescence intensity measurement. To quantify the intracellular delivery efficiency of NBMP-based PINs, flow cytometry was utilized to detect the fluorescence of BODIPY at the AF647 channel (ACEA NovoCyte Quanteon).

Cargo translocation efficiency into the cytosol was determined by the delivery of hydrophobic fluorescent dye, Ce6, and rhodamine B–labeled ovalbumin (rOVA) with green light-responsive BMP. OVA was labeled with rhodamine B isothiocyanate. Briefly, 100 μL of rhodamine B isothiocyanate DMSO solution was dropwise added to 1 mL of 10 mg/mL OVA dissolved in PBS buffer. The mixture was stirred at room temperature in the dark for 1 hour. After that, the labeled OVA was purified by dialysis (MW cutoff: 3,500 Da) against PBS buffer under stirring at 4°C. The PBS buffer was changed frequently until no obvious fluorescence was detected in the dialysis buffer. Then, the labeled OVA was dialyzed against ddH_2O and finally obtained by lyophilization. RAW264.7 cells were incubated with free drugs, PAMAM/rOVA&Ce6 complexes, or HA/BMP-rOVA&Ce6 NPs. The light-treated cells received light irradiation immediately after the addition of NPs into the culture medium. After 4 hours of incubation, intracellular accumulation of rOVA and Ce6 was visualized by confocal laser scanning microscopy (CLSM; LSM 980, Carl Zeiss). rOVA and Ce6 were observed at the AF568 channel and the Qdot655 channel, respectively.

Endosomal escape

To investigate whether light irradiation and BMP can promote endo/lysosomal escape of OVA, RAW264.7 cells were incubated with HA/BMP-rOVA NPs and immediately irradiated by a xenon lamp (520 nm, 25 mW/cm^2, 20 minutes). After 2 hours of incubation, the NP-containing medium was changed to fresh medium. LysoTracker Deep Red was used to label acidic compartments including endosome and lysosome. Cell nuclei were stained by Hoechst 33342. After 0.5, 2, and 4 hours, colocalization of rOVA and LysoTracker Deep Red was monitored under a confocal laser scanning microscope. Hoechst and LysoTracker Deep Red were detected at the 4',6-diamidino-2-phenylindole (DAPI) channel and the AF647 channel, respectively.

Fluorescence resonance energy transfer measurement

The excitation spectrum of rhodamine B overlaps with the emission spectrum of the NIR-responsive photoremovable protecting group (PPG), BODIPY. Therefore, the interaction between OVA and NIR-BODIPY was detected by the fluorescence resonance energy transfer effect. Briefly, the fluorescence spectra (Ex: 520 nm, Em: 560–700 nm) of rOVA, rOVA&NBMP mixture, and OVA&NBMP mixture were measured using a UV-Vis spectrometer (SpectraMax M4, Molecular Device).

Cytotoxicity of PINs on RAW264.7 cells

Cytotoxicity of PINs was tested on RAW264.7 cells. Briefly, PIN with different concentrations determined by BMS986299 was incubated with RAW264.7 cells. Light irradiation was immediately applied after the addition of PIN for the light-treated group. After overnight incubation, the 3-(4,5-dimethylthiazol-2-yl)-2,5 diphenyl tetrazolium bromide assay was conducted to quantify cell viability.

Animal ethics

The study protocol was performed in accordance with the provisions of the Helsinki Declaration of 1975 and was approved by the Institutional Review Board of the University of Hong Kong (IRB approval no.: UW_11–099). Written informed consent was obtained from all subjects. All mouse experiments were approved by the Committee on the Use of Live Animals of HKU (CULATR No. 4617-18).

Tumor models and PIN administration

The OVA-B16F10 melanoma model was developed by s.c. injection of 1×10^6 tumor cells into the flank of C57BL/6 mice (RRID: IMSR_JAX:000664, female, 6–8 weeks old, 18–20 g). When the average volume of tumors reached 50 to 100 mm^3, PINs were administered by i.v. injection for cancer treatment.

For the construction of the mouse orthotopic liver cancer model, we implanted the tumor tissue cubes into the left liver lobes of C57BL/6 mice as described previously (33). Briefly, OVA-RIL-175 cells (1×10^6) in 0.2 mL culture medium were injected subcutaneously into the right flank of each C57BL/6 mouse. Once the subcutaneous tumors reached 0.8 to 1 cm in diameter, they were removed and cut into cubes 1 to 2 mm^3 in size, which were then implanted into the left liver lobes of each C57BL/6 mouse. PINs were administered by i.v. injection for cancer treatment 7 days after tumor implantation.

In vivo PIN biodistribution investigation

When the average volume of the OVA-B16F10 tumor reached 400 mm^3, the tumor-bearing mice were administered with PINs by i.v. injection. The tumor sites were irradiated with NIR light (laser, 660 nm, 100 mW/cm^2, 5 minutes) immediately after PIN administration. After light irradiation, the accumulation of PINs was monitored by an *in vivo* imaging system (IVIS) at the AF647 channel. After 24 hours, the mice were sacrificed, and major organs were collected to analyze the biodistribution of PINs.

The luciferase-expressing OVA-RIL-175 cells were constructed by lentivirus transfection of the luciferase gene into OVA-RIL-175 cells. After the orthotopic tumor implantation, the growth of the OVA-RIL-175 tumor was monitored by IVIS after i.p. injection of D-Luciferin potassium salt. For *in vivo* biodistribution investigation, the sites with the highest luminescence intensity were irradiated with NIR light followed by PIN administration. After light

irradiation, the mice were sacrificed, and major organs were collected for biodistribution analysis.

In vivo antitumor efficacy of PINs

The OVA-B16F10 mice were randomly divided into six groups when the average tumor volume reached 50 to 100 mm^3. The six groups were treated with different formulations via i.v. injection of saline, free BMS and OVA, PIN (mice treated with or without light irradiation), HA/NBMP-OVA NPs (HNONP; mice treated with light irradiation), and HA/NBMP-BMS NPs (HNBNP; mice treated with light irradiation). Light irradiation (laser, 660 nm, 100 mW/cm^2, 5 minutes) was immediately applied at the tumor sites after drug administration. Different formulations were administered on days 7, 10, and 13. The dosage of BMS986299 and OVA was 0.9 mg/kg and 3.6 mg/kg, respectively. Tumor volumes were measured every other day. The mice were sacrificed after the tumor volumes reached the endpoint. Major organs of the mice were collected for biosafety analysis by hematoxylin and eosin (H&E) staining. Tumor tissues were harvested and processed for staining with antibodies to analyze intratumoral infiltration of lymphocytes.

To investigate the antitumor efficacy of PIN and anti-PD-1 combination therapy, OVA-B16F10 tumor-bearing mice were divided into four groups, administered with saline, PINs, anti-PD-1 antibody, and both PIN and anti-PD-1 antibody. Mice treated with PINs were given light irradiation at the tumor sites. PIN was administered on days 7, 14, and 21 through i.v. injection with the same dosage. Anti-PD-1 antibody (clone RMP1-14, Bio X Cell) was administered by i.p. injection with a dosage of 200 μg/mouse on days 9, 11, 16, and 18. The tumor volumes were recorded every other day. For tumor rechallenging experiments, mice were i.v. injected 5×10^5 OVA-B16F10 tumor cells after treatment, lungs were collected and imaged using a smartphone, and the number of tumor nodules was counted. After that, lung tissues were stained by H&E to evaluate lung metastasis of OVA-B16F10 melanoma cells. The multiplex immunofluorescence staining was conducted according to the protocol provided in the Opal 6-Plex Manual Detection Kit by the manufacturer.

To investigate the general applicability of our strategy to another kind of tumor, the orthotopic RIL-175 HCC mouse model was prepared. OVA-RIL-175 carcinoma-bearing mice were also divided into four groups administered with saline, PINs, anti-PD-1 antibody, and both PINs and anti-PD-1 antibody. For tumor rechallenging experiments, mice were i.v. injected 1×10^5 OVA-RIL-175 tumor cells after treatment, lungs were collected and imaged by IVIS to visualize tumor tissues. After that, lung tissues were stained by H&E to evaluate lung metastasis of OVA-RIL-175 HCC cells.

Data availability

All raw data generated in this study are available upon request from the corresponding authors.

Results

PINs enhanced intracellular delivery of BMS986299 and OVA antigens *in vitro*

G5 PAMAM has a well-defined molecular weight and a flexible structure (34), which has been widely studied for cancer imaging and therapies mainly by virtue of multiple functional groups on its surface (35). Notably, PAMAM can act as an adjuvant in drug delivery systems to facilitate antitumor immune responses (36, 37). In this study, NIR light-responsive PPGs, a BODIPY derivative (38), were chemically conjugated to G5 PAMAM to prepare the photo-enhanceable carrier for the NV. The synthesis route of NBMP is shown in Supplementary Fig. S1, and ^{1}H-nuclear magnetic resonance spectra demonstrated the successful synthesis of the dendrimer (32). After BODIPY modification, the grafting number of BODIPY PPGs in one PAMAM was determined as 68.4 by UV-Vis spectroscopy. Our previous findings revealed that BMP exhibited robust efficiency for photo-enhanced intracellular delivery of proteins (39) and small molecules (32). This study is the first attempt to achieve the codelivery of a hydrophilic protein and a hydrophobic small molecule with NBMP and fabrication of the PIN. As expected, NBMP was able to self-assemble with OVA and BMS, separately, to form NPs (Supplementary Fig. S2), which reflected the general applicability of this carrier. To investigate the interaction between NBMP and OVA, rOVA was mixed with NBMP to evaluate the fluorescence resonance energy transfer effect. As shown in Supplementary Fig. S3, the overlap of the rhodamine B emission spectrum and the BODIPY excitation spectrum led to an obvious fluorescence decrease of rhodamine B in the mixture, implying close interactions between OVA and NBMP for self-assembly. The subsequent work focused on preparation of the PINs, i.e., encapsulating both OVA and BMS in NBMP-based NPs. Because of abundant positive charge from unmodified amine groups on NBMP, HA was utilized to coat the NPs to protect them from being endocytosed and ensure the stability during circulation. As shown in **Fig. 1A** and **B**, OVA and BMS formed well-dispersed NPs with NBMP, of which, size and polydispersity index (PdI) were 138.3 nm and 0.193, respectively, after HA coating. The encapsulation efficiencies of BMS and OVA were 26.32% and 21.23%, respectively. And the loading contents of BMS and OVA were 4.83% and 14.59%. Under a transmission electron microscope, the NPs displayed a spherical structure (**Fig. 1C**). Importantly, the NPs kept stable in DMEM complete medium without aggregation (size < 200 nm) and PdI change (<0.3) within 48 hours, which ensured that PINs could be stable during long-time circulation before light irradiation (Supplementary Fig. S4). We then characterized photoresponsiveness of PINs via morphology and zeta potential change measurement. The NIR-responsive BODIPY PPG has a maximum absorption at around 660 nm (Supplementary Fig. S5). As a result, 660 nm light was selected to trigger BODIPY photocleavage from NBMP. Before light irradiation, PINs were negatively charged due to HA coating (**Fig. 1D**). In response to 660-nm light irradiation, PINs dissociated into positively charged fragmented complexes because of photocleavage of BODIPY and re-exposure of amino groups (**Fig. 1C** and **D**). This charge reversal process may promote intracellular delivery and tumor penetration of cargos via electrostatic interactions between positively charged NPs and negatively charged cell membrane. Additionally, the size of PINs changed obviously with PdI increase to more than 0.3 after light irradiation. Through in-tube release experiments, it was found that light irradiation promoted BMS release, thereby activating the signaling pathway. However, OVA release was impeded after light irradiation. This may facilitate more protein penetration through the cell membrane with the help of the vehicle because it is hard for hydrophilic proteins with large size to be transferred into cells (Supplementary Fig. S6). Concisely, we successfully developed a PIN for the codelivery of OVA and BMS. PINs provided us with the possibility to achieve photo-enhanced immunotherapy against tumors.

Intracellular delivery of PINs was monitored by flow cytometry through the fluorescence measurement of the BODIPY PPG. Murine macrophage RAW264.7 cells were incubated with PINs or NIR

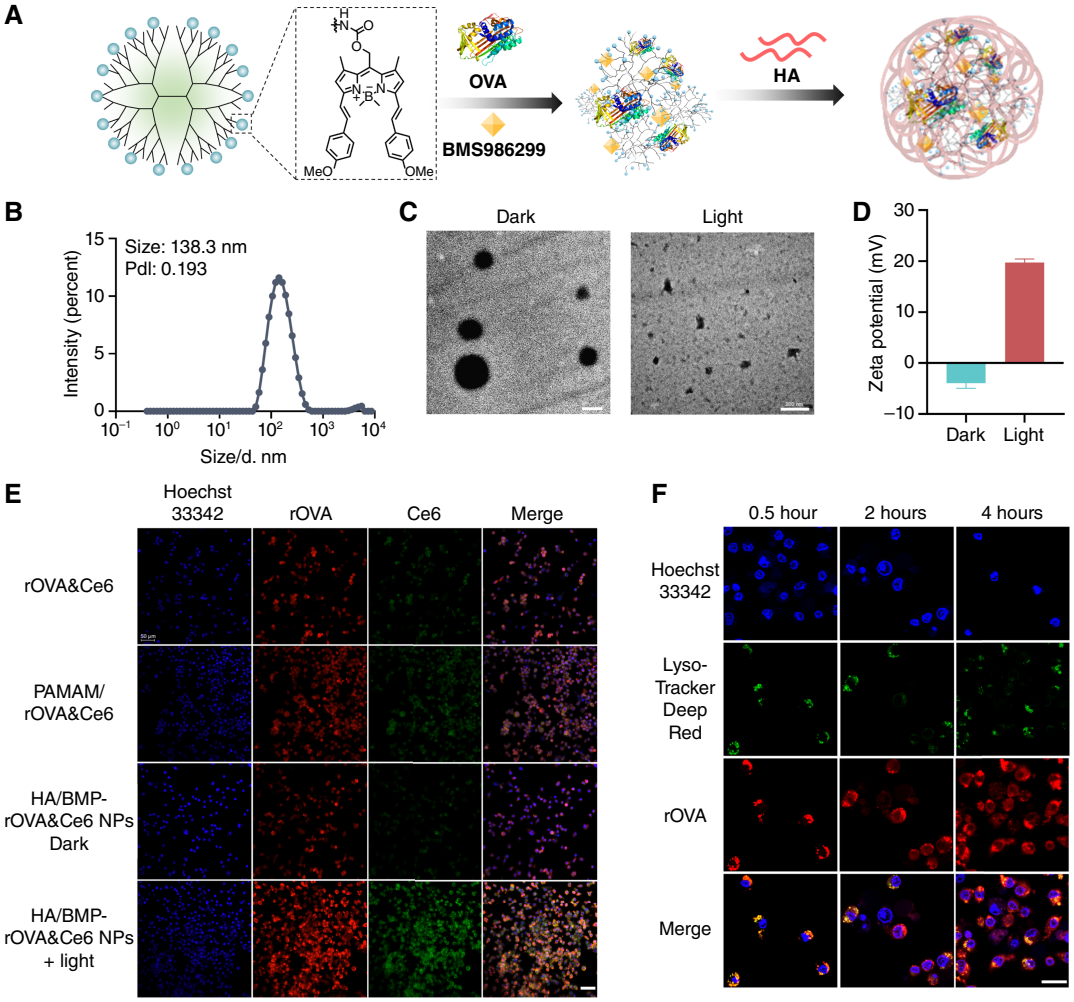

Figure 1.

Characterization of photo-enhanced cellular uptake and endosomal escape of PINs. **A,** Schematic structure of NBMP and preparation of PINs. **B,** Size distribution of PINs measured by dynamic light scattering. **C,** Morphology study of PINs without or with light irradiation using a transmission electron microscope. Scale bar, 200 nm. **D,** Zeta potential measurement of PINs before and after light irradiation. Mean ± SD, $n = 3$. **E,** Comparison of intracellular delivery efficiency of rOVA and fluorescent small molecule Ce6 in various groups: no carrier (rOVA&Ce6), unmodified PAMAM (PAMAM/rOVA&Ce6), BMP without light (HA/BMP-rOVA&Ce6 NPs Dark), BMP with light (HA/BMP-rOVA&Ce6 NPs Light). Scale bar, 50 μm. **F,** Time-dependent monitoring of endosomal escape of rOVA in light-irradiated HA/BMP-rOVA&BMS NP–treated RAW264.7 cells. Endosomes/lysosomes and OVA were labeled by LysoTracker Deep Red and rhodamine B, respectively. Cells were localized by Hoechst 33342. Scale bar, 20 μm. Light irradiation: LED, 660 nm, 100 mW/cm^2, 5 minutes.

light–irradiated PINs. After incubation, cells were harvested for analysis. As shown in Supplementary Fig. S7, light irradiation greatly increased the mean fluorescence intensity of BODIPY in cells, indicating that light irradiation could efficiently enhance the intracellular delivery of PINs, although long-term irradiation could also bleach the fluorescence of BODIPY in the aqueous solution (Supplementary Fig. S8). To further explore the ability of the NBMP system to enhance the transportation of both proteins and small molecules into the cytosol, we prepared NPs encapsulating Ce6, a fluorescent dye, and rOVA. Considering NIR light-responsive BODIPY has overlapped UV-Vis spectra with rhodamine B and Ce6 (Supplementary Fig. S5), we chose green light-responsive BODIPY-modified PAMAM as a tool to study intracellular delivery of proteins and small molecules. As shown in **Fig. 1E,** observed by CLSM, light irradiation significantly promoted intracellular delivery of both rOVA and Ce6 with the assistance of BMP, whereas non-irradiated NPs or the PAMAM/rOVA/Ce6 mixture could not enhance the delivery efficiency compared with free rOVA and Ce6. It is worth noting that RAW264.7 cells treated with nonirradiated NPs showed slightly weaker fluorescence from both rOVA and Ce6 than those treated with free rOVA and Ce6, implying less nonspecific delivery *in vivo* without light irradiation (**Fig. 1E**).

It is crucial for protein-based vaccines to escape endosomes, after which, the vaccines can have access to the cytosolic MHC-I antigen presentation pathway (40). We then, therefore, examined whether BMP promoted endosomal escape of rOVA upon light irradiation by CLSM. After light-irradiated HA/BMP-rOVA&BMS NP incubation, endosomes in treated cells were stained with LysoTracker. Colocalization of rOVA and LysoTracker was utilized to analyze the endosomal escape of rOVA. It was found that rOVA fluorescence

signal initially colocalized with the LysoTracker signal, which means rOVA was entrapped in endosomes after entering cells at the beginning. Then, a time-dependent release of rOVA from the endosome was observed (**Fig. 1F**). The endosomal escape might be explained by the proton-sponge effect mediated by PAMAM (41, 42). To sum up, our findings verified that the BMP system could efficiently promote the uptake of both hydrophilic proteins and hydrophobic small molecules and endosomal escape of OVA to access the MHC-I antigen presentation pathway.

PINs enhanced antigen cross-presentation and NLRP3 activation

The tumor antigens can be processed by proteasomes and other organelles into MHC-I binding peptides (e.g., SIINFEKL), which are consequently presented to $CD8^+$ T cells (43, 44). First, we tested the antigen presentation levels of HNONP-treated cells. In comparison with free OVA and nonirradiated NPs, HNONPs with light irradiation significantly increased SIINFEKL-H2Kb levels on the surface of RAW264.7 cells (**Fig. 2A**). In addition, human serum albumin as an irrelevant antigen was also used here. The HA/NBMP-human serum albumin NPs did not induce MHC-I-SIINFEKL$^+$ Raw264.7 cell proportion increase, indicating that enhanced intracellular delivery of OVA led to the antigen presentation instead of the vehicle. To further monitor antigen cross-presentation ability, HNONP-treated RAW264.7 cells were incubated with SIINFEKL-specific $CD8^+$ T (OT-I) cells to explore whether the strategy could trigger augmented OT-I cell proliferation by an *in vitro* T priming assay. As shown in **Fig. 2B**, HNONPs with light irradiation induced a significantly higher level of OT-I cell proliferation than that induced by the NBMP carrier, free OVA, and HNONPs without light irradiation. Subsequently, we prepared HNBNP to investigate whether our photo-enhanceable NPs could increase the expression levels of proinflammatory IL1β and IL18 because of NLRP3 inflammasome activation mediated by BMS. As shown in **Fig. 2C** and **D**, even at a low BMS concentration (0.08 μmol/L), HNBNPs caused a significant increase in IL1β and IL18 expression upon light irradiation compared with the drug carrier alone or free BMS. These results demonstrated a robust photo-enhanced intracellular delivery capability of NBMP for both OVA and BMS. Therefore, NBMP could promote antigen presentation and IL1β and IL18 expression by elevating intracellular accumulation of OVA and BMS when applying light irradiation. To build a connection between inflammasome activation and antigen presentation, we constructed a coincubation system including different NPs, OVA-expressing melanoma B16F10 (OVA-B16F10) cells, RAW264.7 cells, and OT-I cells to briefly mimic *in vivo* antigen cross-presentation and T cell–mediated killing of tumor cells. The results showed that PINs displayed a robust ability to assist RAW264.7 cells and OT-I cells to kill OVA-B16F10 cancer cells (**Fig. 2E**). It could be explained by enhanced antigen cross-presentation, anticancer cytokine excretion, and OT-I cell activation. Inferior or neglectable anticancer effects were observed when the NPs did not contain OVA or BMS, or RAW264.7 cells and OT-I cells were not involved in this coincubation system (**Fig. 2E**). Importantly, PINs did not show any cytotoxicity on RAW264.7 cells, demonstrating good safety and biocompatibility (Supplementary Fig. S9). This result implied that our strategy could target different processes in the immune response to mediate anticancer effects. Hence, it is important to further explore the *in vivo* effects of PINs to exploit their potential for cancer immunotherapy.

PINs enhanced antitumor immunity in melanoma *in vivo*

Melanoma, the most lethal form of skin cancer, poses significant risks of recurrence and metastasis. Currently, this aggressive tumor is primarily managed through traditional chemotherapy, which is associated with severe adverse effects (45). Hence, developing a precise and effective drug delivery strategy to improve tumor-therapeutic specificity is crucial for melanoma treatment. Photoresponsive drug delivery systems can be utilized suitably in melanoma treatment because light is able to reach melanoma tumor tissues on the skin with high efficiency compared with tumors located deeper within the body. Therefore, we selected OVA-B16F10-melanoma–bearing mice to evaluate the immunotherapy efficacy of our PINs.

First, we tested the *in vivo* targeting ability of our PINs. Because BODIPY is a fluorescent group, we directly detected its fluorescence to evaluate tumor accumulation of PINs. As shown in **Fig. 3A**, we applied NIR light irradiation at the tumor sites immediately after intravenous administration of PINs. The fluorescence distribution of BODIPY was monitored at different time points through the IVIS. We observed that the fluorescence intensity significantly increased at the tumor sites after light irradiation (**Fig. 3B** and **C**), indicating that NIR light–induced charge reversal promoted PIN accumulation in the tumor tissues. Interestingly, we found that the fluorescence gradually increased even after light irradiation (Supplementary Fig. S10). This result might be explained by aggregation-induced fluorescence quenching, whereas the fluorescence increased after penetration and dispersion in tumors. After 24 hours, we sacrificed the tumor-bearing mice and collected tumors and major organs to evaluate biodistribution. It is shown in **Fig. 3B** and **C** that the tumor tissues displayed much stronger fluorescence after PIN administration and light irradiation at the tumor sites. Importantly, no significant PIN residues were found in the major organs of mice (**Fig. 3C**). This result indicated that our strategy could specifically deliver PINs to the tumor tissues to modulate TME without inducing undesired inflammation in normal tissues. With the evidence of light-triggered targeted delivery, we inoculated subcutaneous OVA-B16F10 melanoma cells in the flank of C57BL/6 mice and randomly divided them into six groups, including saline, free BMS&OVA, PINs (dark), HNONPs + light, HNBNPs + light, and PINs + light to investigate the antitumor efficacy of different treatments *in vivo*. The treatment schedule is shown in **Fig. 3D**. Light irradiation was applied at the tumor sites immediately after intravenous administration of NPs. As shown in **Fig. 3E** and **F**, tumor growth was inhibited significantly in the PINs + light group compared with other groups, indicating codelivery of antigen and NLRP3 inflammasome agonist could suppress tumor growth and NBMP as a photoresponsive nanocarrier enhanced such antitumor effects by photo-targeted and photo-enhanced delivery. The tumor volumes in the PINs + light group were consistent with the growth rate curve, showing the best efficacy. Through H&E staining of tumor tissues, more necrosis was also observed in the PINs + light group (Supplementary Fig. S11), indicating more PIN-induced cell deaths in the tumor after light irradiation.

During the treatment, there was no significant difference in body weight among groups before day 13. Afterward, body weight in different groups started to decrease due to the tumor growth burden, but the body weight in the PINs + light group remained the highest, indicating good safety and the highest tumor inhibition efficacy of PINs compared with other groups (Supplementary Fig. S12). Moreover, as shown in Supplementary Fig. S13, no obvious histologic damage and no significant difference between the PIN group and the control group were found in the H&E staining

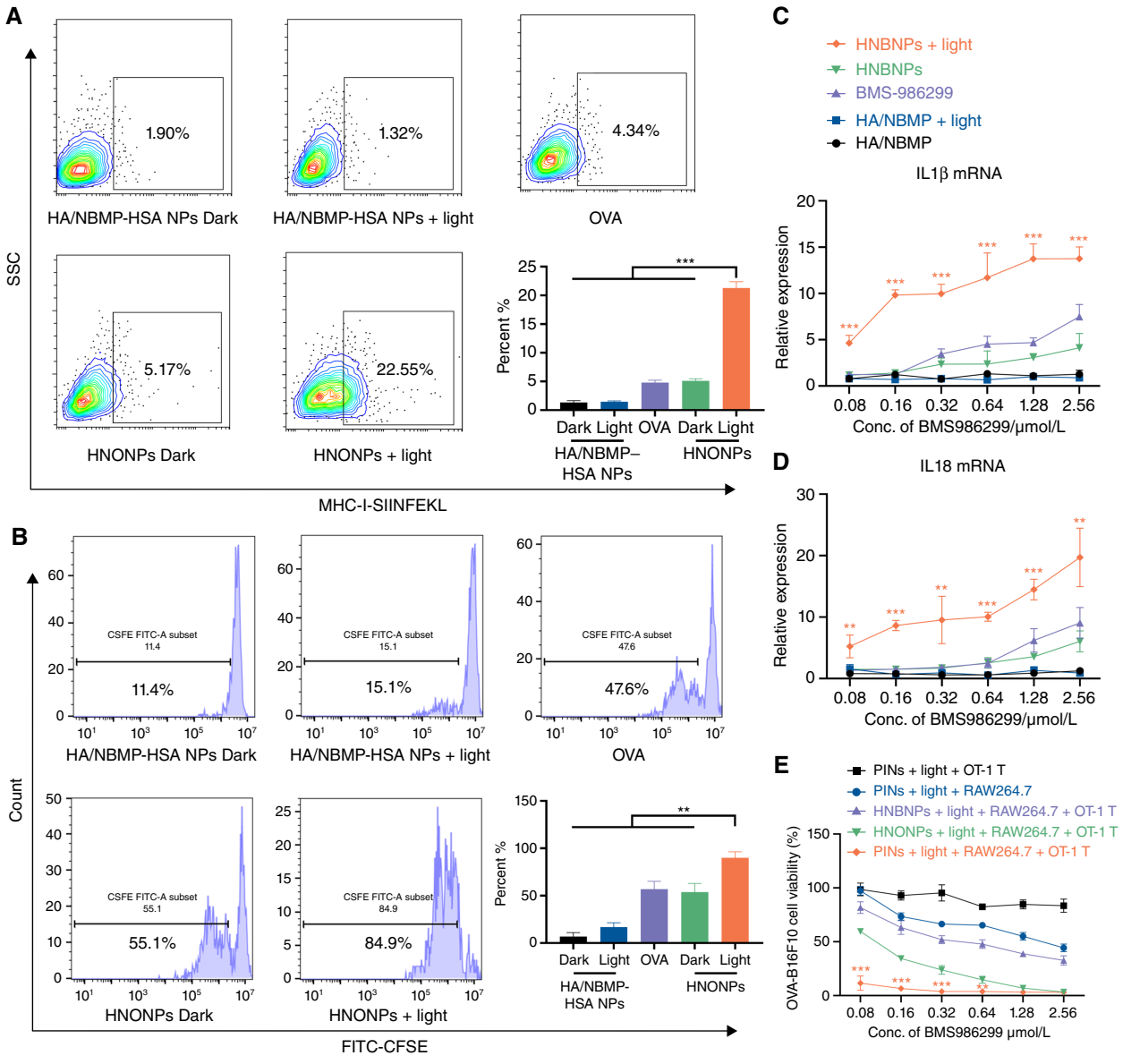

Figure 2.

Photo-enhanced delivery of OVA and BMS for improved antigen presentation, T-cell proliferation, and inflammatory cytokine expression. **A,** Representative flow cytometry data and statistical data of proportions of SIINFEKL$^+$ RAW264.7 cells with different treatments. **B,** Representative flow cytometry data and statistical data exhibiting proliferation [carboxyfluorescein succinimidyl ester (CFSE dilution)] of OT-I T cells incubated with RAW264.7 cells with different treatments. **C** and **D,** Transcription levels of IL1β (**C**) and IL18 (**D**) after different treatments. One-way ANOVA was used to compare the significant difference between the HNBNPs + light group and every other group. **E,** Viability of OVA-B16F10 cells coincubated with RAW264.7 cells/OT-I T cells and different NPs. Cell viability was measured using the MTT assay. RAW264.7: OT-I = 1: 4; OT-I: tumor cells (E:T) = 4:1. One-way ANOVA was used to compare the significant difference between the PIN + light + RAW264.7 + OT-I group and every other group. Mean ± SD, $n = 3$. Light irradiation: LED, 660 nm, 100 mW/cm^2, 5 minutes. Statisical method, one-way ANOVA. **, $P < 0.01$; ***, $P < 0.001$.

and liver function tests (alanine aminotransferase and aspartate aminotransferase levels). To explore the mechanisms of anticancer effects from the PINs, activation of the NLRP3 signaling pathway was evaluated. Several NLRP3 markers including cleaved caspase-1, IL18, IL1β, and apoptosis-associated speck-like protein containing a caspase recruitment domain (ASC) were visualized by immunofluorescence staining. The results in Supplementary Fig. S14 show that caspase-1, IL18, IL1β, and ASC were highly expressed in HNBNPs + light and PINs + light groups, suggesting BMS-induced higher NLRP3 pathway activation after treatment. The Western blotting analysis of NLRP3, caspase-1, and cleaved caspase-1 (Supplementary Fig. S15) from OVA-B16F10 tumors of treated mice also provided evidence on NLRP3 activation. The NLRP3 increased significantly with the treatment of PINs and light irradiation,

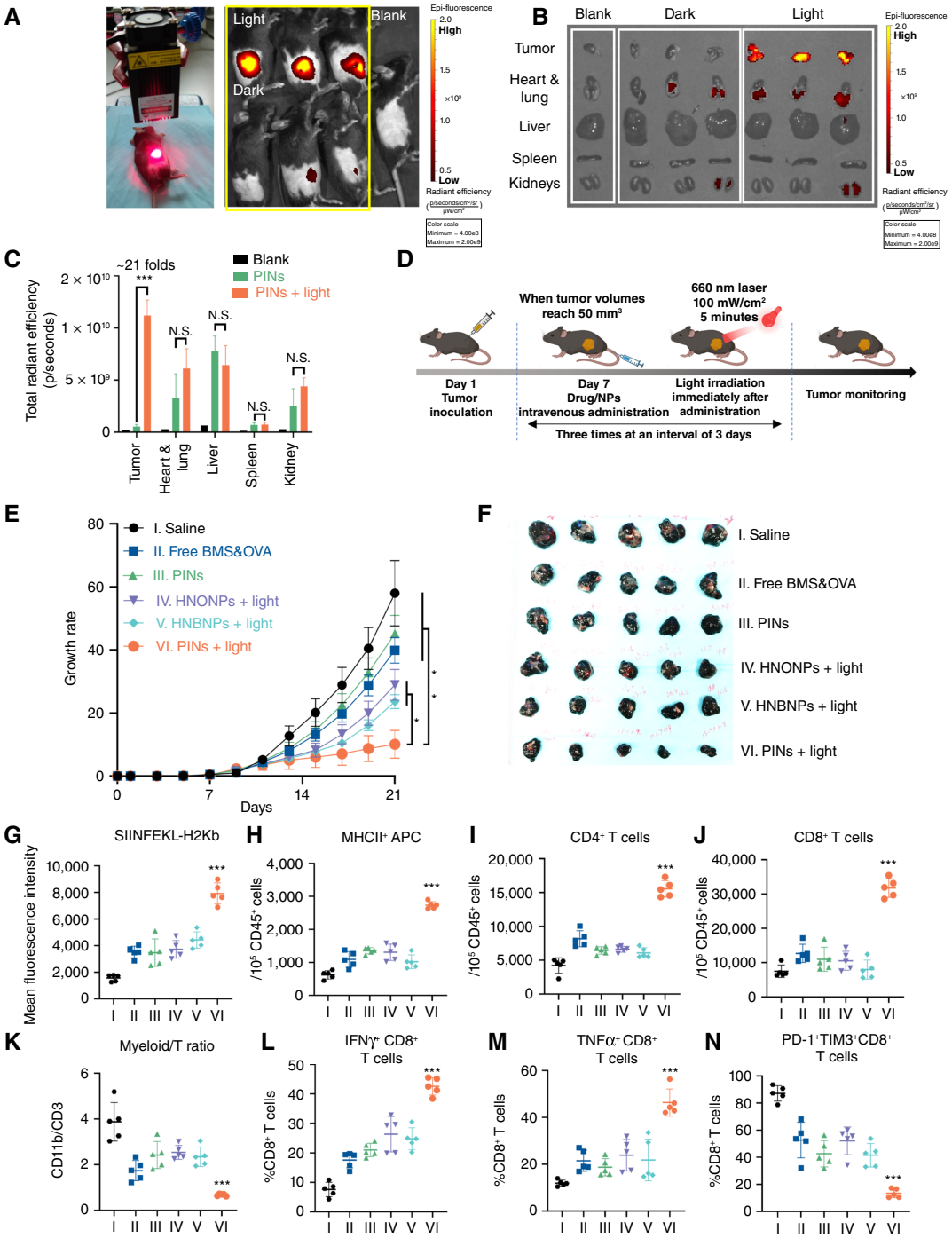

Figure 3.

Photo-enhanced PIN delivery for subcutaneous OVA-B16F10 melanoma model and immune effects. **A,** Light irradiation applied at tumor sites and accumulation of PINs in tumors. Fluorescence from BODIPY measured by PerkinElmer IVIS Lumina was utilized to determine PIN accumulation. Channel: AF647. **B,** Detection of BODIPY fluorescence in collected tumors and major organs from sacrificed mice with PIN administration with or without light irradiation. **C,** Statistical data of fluorescence distribution in tumors and major organs. Mean ± SD, $n = 3$. **D,** Treatment schedule of PIN therapy in tumor-bearing C57BL/6 mice. **E,** Tumor growth monitoring in the OVA-B16F10 melanoma mouse model treated with saline, free BMS&OVA, HNO-NPs + light irradiation, HNB-NPs + light irradiation, and PINs −/+ light irradiation, separately. Mean ± SEM, $n = 5$. Statistical method, t test. **F,** Photo of collected tumor tissues after sacrificing mice from different groups. **G–N,** Statistical data of flow cytometry analysis of tumor-infiltrated $CD45^+CD3^-CD19^-CD11C^+$SIINFEKL-$H2Kb^+$ APCs (**G**), $CD45^+CD19^-CD3^-CD11b^+MHCII^+$APCs (**H**), $CD45^+CD3^+CD4^+$ T cells (**I**), $CD45^+CD3^+CD8^+$ T cells (**J**), ratio of $CD45^+CD11b^+$ myeloid cells to $CD4^+CD3^+$ T cells (**K**), $CD45^+CD8^+IFN\gamma^+$ T cells (**L**), $CD45^+CD8^+TNF\alpha^+$ T cells (**M**), and $CD45^+CD8^+PD\text{-}1^+TIM3^+$ T cells (**N**). Mean ± SD, $n = 5$. Statistical method, one-way ANOVA. Light irradiation: laser, 660 nm, 100 mW/cm², 5 minutes. N.S., nonsignificant; *, $P < 0.05$; ***, $P < 0.001$.

leading to a higher level of cleaved caspase-1. However, caspase-1 level did not change, further indicating that the treatment promotes NLRP3 activation instead of expression level increase in caspase-1. NLRP3 activation could modulate TME toward inflammation and mobilize anticancer immunity. Therefore, we then quantified tumor-infiltrated lymphocytes to characterize TME, and the gating strategy is shown in Supplementary Fig. S16. Notably, PINs + light treatment resulted in the highest level of $CD11c^+SIINFEKL\text{-}H2Kb^+$ APCs infiltrated in the tumors (**Fig. 3G**; Supplementary Fig. S17). As expected, the number of $CD11b^+MHC\text{-}II^+$ APCs also increased significantly in the PINs + light group (**Fig. 3H**; Supplementary Fig. S18). These data indicated that our strategy could significantly enhance the accumulation and intracellular delivery of OVA to APCs in the tumor tissues to induce antigen presentation and T-cell priming. We then analyzed the numbers of $CD8^+$ and $CD4^+$ T cells in tumors. The results showed that higher numbers of $CD4^+$ and $CD8^+$ T lymphocytes were recruited to the tumors with PINs and light treatment compared with other groups (**Fig. 3I** and **J**; Supplementary Figs. S19 and S20). PIN-treated mice also showed a decreased ratio of myeloid cells to T cells (**Fig. 3K**; Supplementary Fig. S21), indicating a T cell–dominant TME in mice with PINs and light treatment. We further analyzed the frequencies of $IFN\gamma^+CD8^+$ T cells and $TNF\alpha^+CD8^+$ T cells by flow cytometry. The results in **Fig. 3L** and **M**; Supplementary Figs. S22 and S23 show that PINs significantly increased the expression of IFNγ and TNFα in $CD8^+$ T cells after light irradiation. Besides, PINs could downregulate the expression of the immune checkpoints, PD-1 and TIM3 (**Fig. 3N**; Supplementary Fig. S24). The IHC staining also showed that the expression of CD8, TNFα, perforin, and granzyme B was significantly increased in tumors with PIN treatment (Supplementary Fig. S25). Taken together, PINs could achieve *in situ* activation of antitumor immunity by simultaneously promoting the activation of NLRP3 inflammasomes and antigen cross-presentation in APCs, ultimately converting the "cold tumor" into the "hot tumor."

PINs enhanced the efficacy of immune checkpoint inhibitor in melanoma and HCC

Although ICB immunotherapy has been widely utilized for cancer therapy (46), the response rates remain dismal, with less than 50% in melanoma (47) and around 15% to 20% in HCC (48) due to the intrinsic immunosuppressive TME (49, 50). As our PINs have been proven to convert "cold tumor" into "hot tumor," we speculated that they can enhance the efficacy of PD-1 inhibitor in cancer treatment. To prove this hypothesis, we applied the OVA-B16F10 melanoma mouse model, in which each C57BL/6 mouse was inoculated with OVA-B16F10 cells with stably expressed OVA protein. PINs were administered by i.v. injection on day 7. NIR light irradiation was immediately applied after administration. Two booster shots were followed on day 14 and day 21. Mice from the anti-PD-1 group and the combination group received anti-PD-1 antibody on days 9, 11, 16, and 18 by i.p. injection (**Fig. 4A**). Tumor growth of each mouse was monitored every other day, as shown in **Fig. 4B**. As expected, PIN treatment significantly inhibited tumor growth compared with the saline group. Importantly, PIN and anti-PD-1 combination therapy exhibited the best tumor growth inhibition in comparison with a single PIN or single anti-PD-1 treatment (**Fig. 4C**). The combination therapy also extended the survival time of OVA-B16F10 tumor-bearing mice (**Fig. 4D**).

After exhibiting the outstanding performance of our PINs in the melanoma model, we further explored whether our strategy is reproducible in an intra-abdominal tumor model. The immunotherapy-resistant murine HCC cells, OVA-RIL-175 with luciferase expression were inoculated into mouse liver to construct a mouse model with orthotopic liver cancer. PINs were administered by i.v. injection from the tail vein, and light irradiation was applied at the tumor sites labeled through IVIS. After light irradiation, we used IVIS to monitor the fluorescence distribution to track drug accumulation in the tumor tissues. As shown in **Fig. 5A**, much stronger fluorescence from BODIPY was observed in the tumor sites irradiated by light than in those without light irradiation. Importantly, only a small amount of PINs were found in major organs of mice, indicating a highly specialized targeting ability of PINs with the assistance of light. We further investigated whether PINs could enhance the efficacy of anti-PD-1 immunotherapy against HCC. The mice in the anti-PD-1 antibody group and the combination therapy group received anti-PD-1 antibody by i.p. injection. The treatment schedule was the same as in **Fig. 4A**. Then, tumor growth was monitored through luminescence intensity measurement by IVIS. It is shown in **Fig. 5B** and **C** that PIN and anti-PD-1 combination therapy significantly inhibited tumor growth, whereas single PIN treatment or anti-PD-1 antibody treatment only exhibited limited tumor-killing efficacy. Furthermore, the combination therapy significantly extended the survival time of OVA-RIL-175 tumor-bearing mice (**Fig. 5D**). These results suggested that our nanocarrier could selectively deliver OVA and BMS to the tumor sites in the liver with the help of NIR light. Therefore, our data suggested that PINs could enhance the immunotherapy efficacy of PD-1 blockade.

PINs induced long-term immune memory against tumors

To explore whether our strategy could establish long-term immune memory against tumors, we conducted OVA-RIL-175 and OVA-B16F10 tumor rechallenge experiments (**Fig. 6A**). After treatment of PINs and anti-PD-1 mAb, tumor-bearing mice were rechallenged with tumor cells via tail vein injection. The lung tissues of each group were collected 3 weeks after rechallenging. The metastatic tumor nodules on the lungs were observed and quantified by either H&E staining or IVIS. As shown in **Fig. 6B**, the lung metastases significantly decreased in treated mice compared with the untreated mice in the OVA-RIL-175 liver cancer model (**Fig. 6C**). Similarly, in the OVA-B16F10 mouse melanoma model, the treated mice showed much fewer lung metastases than those in the control group (**Fig. 6D** and **E**).

Memory T cells play an important role in preventing cancer metastasis and recurrence (51, 52). To further investigate the immune memory established by PIN and anti-PD-1 combination therapy, multiplex immunofluorescence staining was conducted in the lung tissues of the mice in the control group and combination therapy group. Consistently, more effector memory $CD8^+$ T cells ($TCF1^+CD44^+$) with higher levels of granzyme B expression were found in the lung tissues after the combination therapy in both melanoma and HCC mouse models, as shown in **Fig. 6F** and Supplementary Fig. S26, respectively. Besides, T cell factor-1 (TCF1) is an important transcription factor during T-cell development and differentiation (53) and CD44 is a surface marker of long-lived memory T cells (54). Our result showed increased $TCF1^+CD44^+CD8^+$ T cells in the lung tissues after the treatment **Fig. 6F** and Supplementary Fig. S26. A detailed statistical analysis of $CD8^+$ T cells, $CD8^+TCF1^+$ T cells, and granzyme B in two tumor models (Supplementary Fig. S27) with the above evidence suggested the administration of PINs could establish long-term immune memory against tumors.

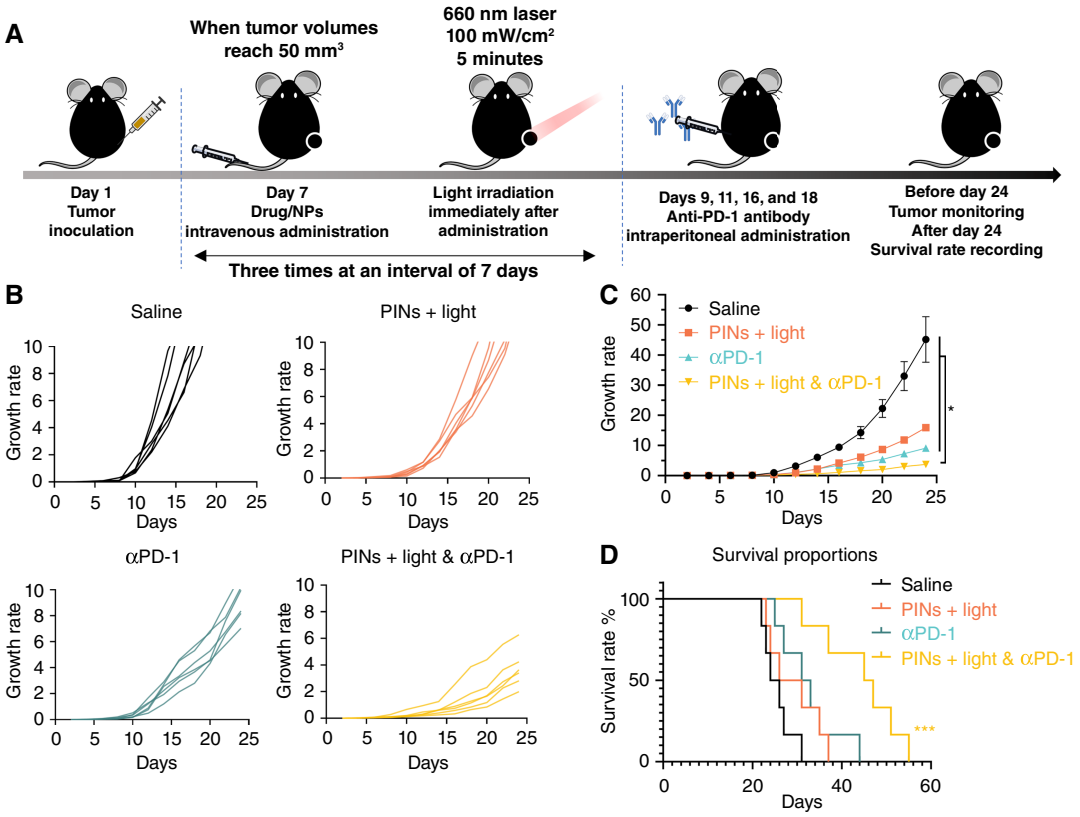

Figure 4.

PIN-enhanced ICB therapy in the subcutaneous melanoma mouse model. **A,** Treatment schedule of PINs and PD-1 inhibitor combination therapy in murine melanoma OVA-B16F10–bearing C57BL/6 mice. **B,** Tumor growth rate curves in different groups. **C,** Mean growth rates of OVA-B16F10 tumor-bearing mice with different treatments. Statistical method, one-way ANOVA. **D,** Survival rate curves of OVA-B16F10 tumor-bearing mice. Statistical method, survival analysis. Light irradiation: laser, 660 nm, 100 mW/cm^2, 5 minutes. *, $P < 0.05$; ***, $P < 0.001$.

Discussion

In conclusion, we report a new strategy to fabricate a PIN. This study, for the first time, incorporated a neoantigen (OVA) and an NLRP3 agonist into PINs to gain a robust immune response against tumors via systematic drug administration and localized tumor irradiation. PINs showed strong anticancer efficacy against melanoma and HCC with robust TME remodeling ability. Such a photo-enhanceable NV can be further personalized for different types of cancer by incorporating corresponding neoantigens into the PINs for clinical translation.

In detail, we developed a photoresponsive dendrimer, BMP. Such BMP self-assemble with a hydrophilic protein antigen, OVA, and a hydrophobic immunologic adjuvant, BMS by simply mixing to form PINs with a uniform size. Under NIR light irradiation at the tumor sites, PINs could accumulate at the tumor tissues with high targeting efficiency based on photo-triggered charge reversal. PINs showed superior efficiency in TME remodeling by facilitating antigen cross-presentation and TME inflammation after light irradiation due to photo-enhanced intracellular delivery of OVA and BMS. Without treatment of PINs, less infiltration of proinflammatory and cytotoxic immune cells was attributed to immunosuppressive TME, whereas PINs were proven to inhibit melanoma growth upon light irradiation by promoting antigen cross-presentation, cytotoxic T-cell infiltration, and anticancer cytokine secretion because of successful tumor antigen delivery to APCs and NLRP3 inflammasome activation in TME. Importantly, we found in our study that such TME remodeling by PINs could amplify the antitumor immune response of ICB as demonstrated in the subcutaneous melanoma model and the orthotopic carcinoma model. Furthermore, we observed a strong immune memory effect to effectively protect tumor-bearing mice from tumor rechallenge.

Traditional NVs were administered by s.c. or intramuscular injection to activate the immune system. This study provided a new approach to NV administration through i.v. injection. In addition, studies have demonstrated that the coadministration of adjuvants with antigens significantly enhances antigen processing in APCs (25, 55, 56), but *in situ* delivery of both tumor antigens and proinflammatory immune adjuvant is challenging in most NVs. Meanwhile, immunosuppression in TME cannot be directly overcome with the treatment of such NVs. On the contrary, PINs with the inflammasome agonist can selectively accumulate in the tumor tissues with the help of light for efficient TME conversion. In this case, the efficacy of cargo drugs in PINs can be ensured and abnormal inflammation in normal tissues can be avoided, whereas previous NVs may cause off-targeted delivery and induce side effects. Although many *in situ* tumor NVs showed promise for cancer prevention and treatment by triggering immunogenic cell death and

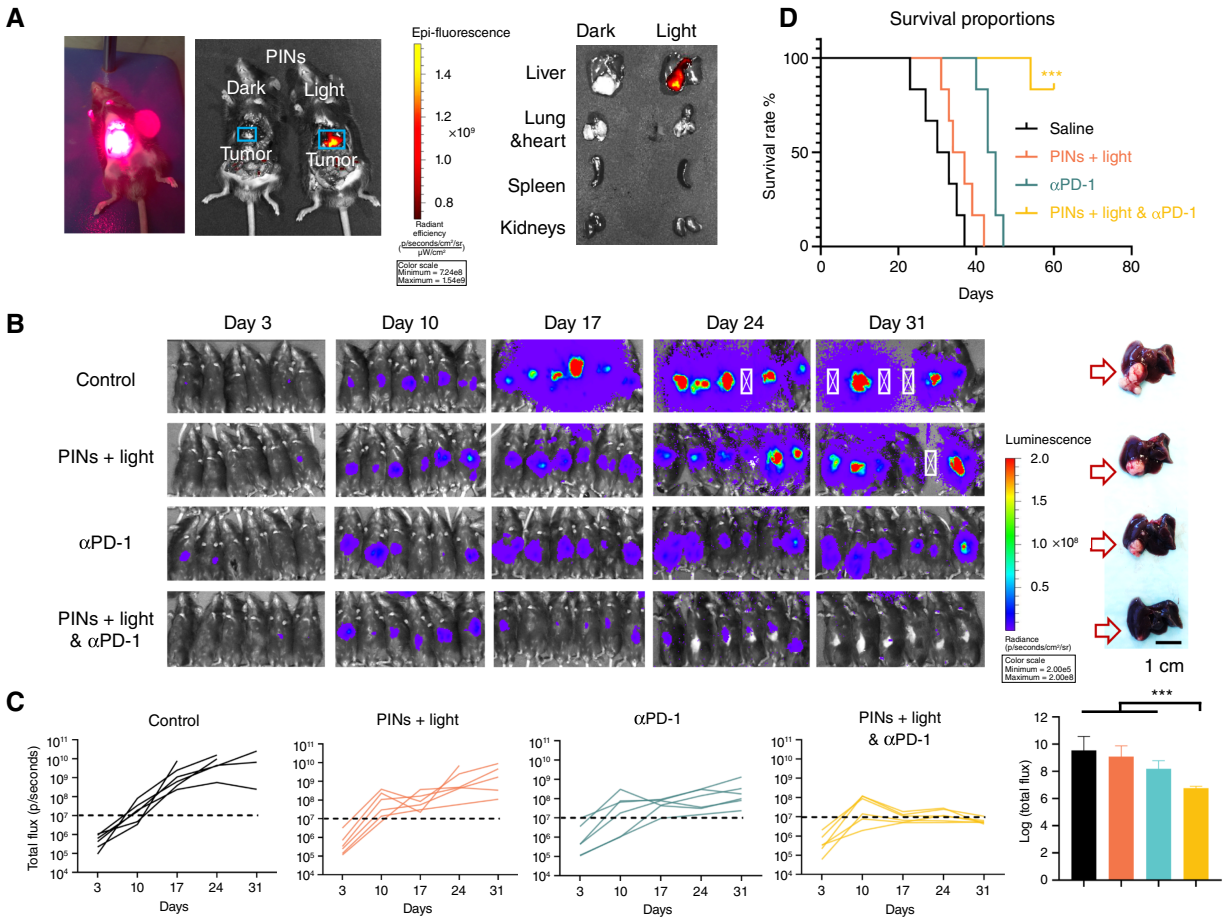

Figure 5.

PIN-enhanced ICB therapy in the orthotopic HCC mouse model. **A,** Light irradiation applied at the liver sites with murine HCC OVA-RIL-175 and accumulation of PINs in tumors after light irradiation. Major organs were collected after sacrificing the tumor-bearing mice to detect BODIPY fluorescence. Channel: AF647. **B,** Bioluminescence images of HCC OVA-RIL-175-bearing mice (i.e., luciferase-expressing OVA-RIL-175 cells) after treatment of saline, PINs + light, anti-PD-1 antibody (αPD-1), and PINs + light and αPD-1. Right, representative photo of tumors from each group. Scale bar, 1 cm. **C,** Statistics of luminescence intensity from luciferase-expressing OVA-RIL-175 tumor-bearing mice administered with luciferin. Statistical method, one-way ANOVA. **D,** HCC OVA-RIL-175-bearing mouse survival rate curves. Statistical method, survival analysis. Light irradiation: laser, 660 nm, 100 mW/cm^2, 5 minutes. ***, $P < 0.001$.

immune activation, limited intracellular translocation and low cross-presentation of tumor antigens limit the therapeutic efficacy. PINs can enhance the intracellular delivery efficiency and endosome escape of tumor antigens for high antigen cross-presentation levels under light irradiation.

PINs offer several advantages in cancer treatment. First, they enable precise localized therapy by targeted drug release, minimizing damage to healthy tissues and enhancing safety. Second, PINs can be controlled using external light sources, allowing real-time treatment adjustments, and increasing treatment controllability and flexibility. Most importantly, the drug delivery strategy used in PINs could reduce treatment side effects, enhancing the quality of life for patients. Therefore, PINs hold promise as an innovative, efficient, and low-risk approach to cancer treatment. Several limitations need to be acknowledged. First, whereas the study indicated good biocompatibility and safety of PINs in mice, the potential long-term toxicity and immune reactions in humans need thorough evaluation. Second, tumors in patients are often heterogeneous, and our study utilized OVA as a model antigen, which may not accurately represent the complexity of tumor-specific antigens found in human cancers. Therefore, more personalized approaches for antigen selection might be needed, and the efficacy of PINs in addressing this heterogeneity needs further investigation as well. Lastly, despite the favorable therapeutic effects of PINs in orthotopic liver cancer, their clinical applicability might be constrained for tumors situated at greater depths within the body with denser surrounding tissue architecture, such as glioblastomas and retroperitoneal tumors, due to the limited penetration ability of available light wavelengths. In the future, more PPGs with longer wavelength responsiveness can be further used to increase light penetration for more applications. Meanwhile, ultrasound possesses remarkable depth penetration capabilities, and there is potential for further exploration of ultrasound-enhanced intracellular drug delivery based on similar mechanisms to broaden its applications in biochemistry. Additionally, more wearable light sources or implantable optical fiber will be used for

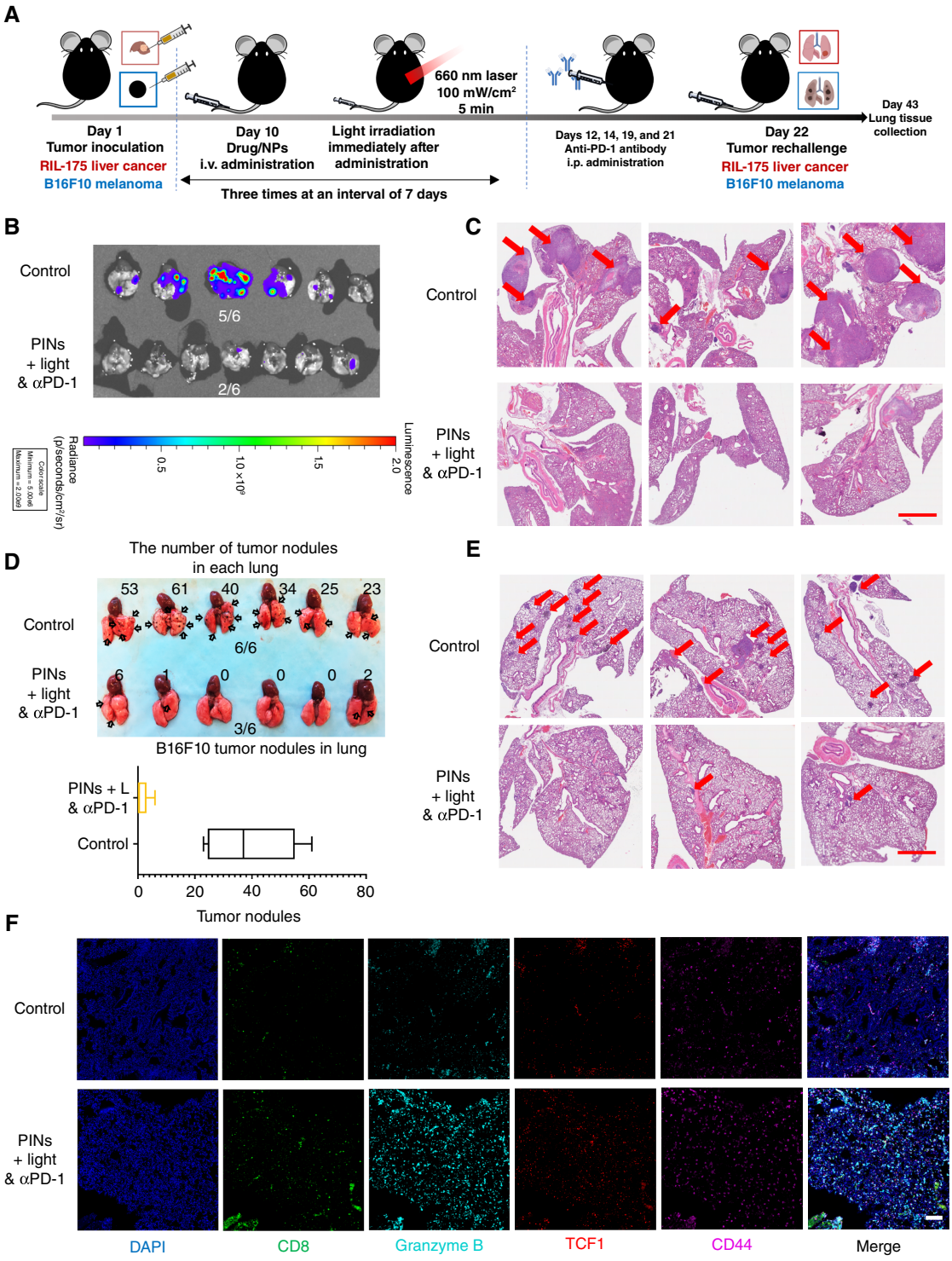

Figure 6.

Tumor rechallenge after combination therapy with PINs and PD-1 inhibitor. **A,** Treatment schedule of PINs and PD-1 inhibitor combination therapy in OVA-B16F10 and OVA-RIL-175–bearing C57BL/6 mice. **B** and **C,** Bioluminescence images of collected lungs (**B**) and H&E staining of lung tissues (**C**) from OVA-RIL-175 rechallenged C57BL/6 mice. Scale bar, 800 μm. **D** and **E,** Photo of lung tissues (**D**) and H&E staining of lung tissues (**E**) from OVA-B16F10 rechallenged C57BL/6 mice. Tumor nodules were counted for statistical analysis. Mean ± SD, $n = 6$. Scale bar, 800 μm. **F,** Multiplex immunofluorescence staining of lung tissues from OVA-RIL-175 tumor-bearing and rechallenged mice without treatment or with the treatment of PINs + light and αPD-1. Scale bar, 100 μm. Light irradiation: laser, 660 nm, 100 mW/cm^2, 5 minutes.

light delivery in deep tissues with the rapid development of bioengineering technology.

In conclusion, our study proposed a new concept of photoenhanceable personalized cancer vaccines based on the photoresponsive BMP dendrimer. We believe that BMP can be further used to achieve photo-enhanced intracellular delivery of hydrophilic and hydrophobic cargos simultaneously for different diseases. As a proof of concept, our study provides a novel, safe, and efficient photoresponsive drug delivery system that demonstrated simultaneous delivery of antigen and immune-modulating small molecule into tumor tissues with high therapeutic efficacy.

Authors' Disclosures

No disclosures were reported.

Authors' Contributions

Y. Zhou: Conceptualization, data curation, formal analysis, investigation, methodology, writing–original draft, project administration. **L. Pang:** Conceptualization, data curation, funding acquisition, investigation, methodology, project administration, writing–review and editing. **T. Ding:** Software, formal analysis, validation, investigation, methodology, writing–review and editing. **K. Chen:** Investigation, methodology. **J. Liu:** Investigation, methodology, writing–review and editing. **M. Wu:** Investigation. **W. Wang:** Conceptualization, resources, supervision, funding acquisition, methodology, project administration. **K. Man:** Conceptualization, resources, supervision, funding acquisition, methodology, project administration, writing–review and editing.

Acknowledgments

We acknowledge the assistance of the Faculty Core Facility of Li Ka Shing Faculty of Medicine, The University of Hong Kong. W. Wang was supported by the National Natural Science Foundation of China (no. 82222903); K. Man was supported by Theme-based Research Scheme of Hong Kong (T12-703/19R); L. Pang was supported by the National Natural Science Foundation of China (no. 82203747) and China Postdoctoral Science Foundation (no. 2022TQ0388 and 2023M734036).

Note

Supplementary data for this article are available at Cancer Research Online (http://cancerres.aacrjournals.org/).

Received January 22, 2024; revised July 4, 2024; accepted September 11, 2024; published first September 17, 2024.

References

1. Weiss SA, Wolchok JD, Sznol M. Immunotherapy of melanoma: facts and hopes. Clin Cancer Res 2019;25:5191–201.
2. Mamdani H, Matosevic S, Khalid AB, Durm G, Jalal SI. Immunotherapy in lung cancer: current landscape and future directions. Front Immunol 2022;13:823618.
3. Daver N, Alotaibi AS, Bücklein V, Subklewe M. T-cell-based immunotherapy of acute myeloid leukemia: current concepts and future developments. Leukemia 2021;35:1843–63.
4. Hegde PS, Chen DS. Top 10 challenges in cancer immunotherapy. Immunity 2020;52:17–35.
5. Sambi M, Bagheri L, Szewczuk MR. Current challenges in cancer immunotherapy: multimodal approaches to improve efficacy and patient response rates. J Oncol 2019;2019:4508794.
6. Tang H, Qiao J, Fu Y-X. Immunotherapy and tumor microenvironment. Cancer Lett 2016;370:85–90.
7. Sadeghi Rad H, Monkman J, Warkiani ME, Ladwa R, O'Byrne K, Rezaei N, et al. Understanding the tumor microenvironment for effective immunotherapy. Med Res Rev 2021;41:1474–98.
8. Xu J, Lv J, Zhuang Q, Yang Z, Cao Z, Xu L, et al. A general strategy towards personalized nanovaccines based on fluoropolymers for post-surgical cancer immunotherapy. Nat Nanotechnol 2020;15:1043–52.
9. Xu J, Wang H, Xu L, Chao Y, Wang C, Han X, et al. Nanovaccine based on a protein-delivering dendrimer for effective antigen cross-presentation and cancer immunotherapy. Biomaterials 2019;207:1–9.
10. Zhu G, Zhang F, Ni Q, Niu G, Chen X. Efficient nanovaccine delivery in cancer immunotherapy. ACS Nano 2017;11:2387–92.
11. Zhang D, Lin Z, Wu M, Cai Z, Zheng Y, He L, et al. Cytosolic delivery of thiolated neoantigen nano-vaccine combined with immune checkpoint blockade to boost anti-cancer T cell immunity. Adv Sci (Weinh) 2021;8:2003504.
12. Hammerich L, Marron TU, Upadhyay R, Svensson-Arvelund J, Dhainaut M, Hussein S, et al. Systemic clinical tumor regressions and potentiation of PD1 blockade with in situ vaccination. Nat Med 2019;25:814–24.
13. Yue Y, Xu J, Li Y, Cheng K, Feng Q, Ma X, et al. Antigen-bearing outer membrane vesicles as tumour vaccines produced in situ by ingested genetically engineered bacteria. Nat Biomed Eng 2022;6:898–909.
14. Viswanath DI, Liu H-C, Huston DP, Chua CYX, Grattoni A. Emerging biomaterial-based strategies for personalized therapeutic in situ cancer vaccines. Biomaterials 2022;280:121297.
15. Bo Y, Wang H. Biomaterial-based in situ cancer vaccines. Adv Mater 2023 Jan 17 [Epub ahead of print].
16. Franchi L, Muñoz-Planillo R, Núñez G. Sensing and reacting to microbes through the inflammasomes. Nat Immunol 2012;13:325–32.
17. Sharma BR, Kanneganti T-D. NLRP3 inflammasome in cancer and metabolic diseases. Nat Immunol 2021;22:550–9.
18. Martinon F, Burns K, Tschopp J. The inflammasome: a molecular platform triggering activation of inflammatory caspases and processing of proIL-beta. Mol Cell 2002;10:417–26.
19. Van Den Eeckhout B, Tavernier J, Gerlo S. Interleukin-1 as innate mediator of T cell immunity. Front Immunol 2021;11:621931.
20. Nambu A, Nakae S, Iwakura Y. IL-1beta, but not IL-1alpha, is required for antigen-specific T cell activation and the induction of local inflammation in the delayed-type hypersensitivity responses. Int Immunol 2006;18:701–12.
21. Ghiringhelli F, Apetoh L, Tesniere A, Aymeric L, Ma Y, Ortiz C, et al. Activation of the NLRP3 inflammasome in dendritic cells induces IL-1beta-dependent adaptive immunity against tumors. Nat Med 2009;15:1170–8.
22. He Y, Hara H, Núñez G. Mechanism and regulation of NLRP3 inflammasome activation. Trends Biochem Sci 2016;41:1012–21.
23. Stoll S, Müller G, Kurimoto M, Saloga J, Tanimoto T, Yamauchi H, et al. Production of IL-18 (IFN-gamma-inducing factor) messenger RNA and functional protein by murine keratinocytes. J Immunol 1997;159:298–302.
24. Chaix J, Tessmer MS, Hoebe K, Fuséri N, Ryffel B, Dalod M, et al. Cutting edge: priming of NK cells by IL-18. J Immunol 2008;181:1627–31.
25. Gong N, Zhang Y, Teng X, Wang Y, Huo S, Qing G, et al. Proton-driven transformable nanovaccine for cancer immunotherapy. Nat Nanotechnol 2020;15:1053–64.
26. Lu Y, Xu S, Chen H, He M, Deng Y, Cao Z, et al. CdSe/ZnS quantum dots induce hepatocyte pyroptosis and liver inflammation via NLRP3 inflammasome activation. Biomaterials 2016;90:27–39.
27. Zhang X, Luan J, Chen W, Fan J, Nan Y, Wang Y, et al. Mesoporous silica nanoparticles induced hepatotoxicity via NLRP3 inflammasome activation and caspase-1-dependent pyroptosis. Nanoscale 2018;10:9141–52.
28. Mangan MSJ, Olhava EJ, Roush WR, Seidel HM, Glick GD, Latz E. Targeting the NLRP3 inflammasome in inflammatory diseases. Nat Rev Drug Discov 2018;17:588–606.
29. Long K, Wang Y, Lv W, Yang Y, Xu S, Zhan C, et al. Photoresponsive prodrug-dye nanoassembly for in-situ monitorable cancer therapy. Bioeng Transl Med 2022;7:e10311.
30. Li Y, Zhang Y, Wang W. Phototriggered targeting of nanocarriers for drug delivery. Nano Res 2018;11:5424–38.
31. Rwei AY, Wang W, Kohane DS. Photoresponsive nanoparticles for drug delivery. Nano Today 2015;10:451–67.
32. Zhou Y, Chen K, Lin WK, Liu J, Kang W, Zhang Y, et al. Photo-enhanced synergistic induction of ferroptosis for anti-cancer immunotherapy. Adv Healthc Mater 2023;12:e2300994.

33. Man K, Ng KTP, Xu A, Cheng Q, Lo CM, Xiao JW, et al. Suppression of liver tumor growth and metastasis by adiponectin in nude mice through inhibition of tumor angiogenesis and downregulation of Rho kinase/IFN-inducible protein 10/matrix metalloproteinase 9 signaling. Clin Cancer Res 2010;16:967–77.
34. Tang Y, Han Y, Liu L, Shen W, Zhang H, Wang Y, et al. Protective effects and mechanisms of G5 PAMAM dendrimers against acute pancreatitis induced by caerulein in mice. Biomacromolecules 2015;16:174–82.
35. Li H, Zha S, Li H, Liu H, Wong KL, All AH. Polymeric dendrimers as nanocarrier vectors for neurotheranostics. Small 2022;18:e2203629.
36. Liu J, Li H-J, Luo Y-L, Chen Y-F, Fan Y-N, Du J-Z, et al. Programmable delivery of immune adjuvant to tumor-infiltrating dendritic cells for cancer immunotherapy. Nano Lett 2020;20:4882–9.
37. Chowdhury S, Toth I, Stephenson RJ. Dendrimers in vaccine delivery: recent progress and advances. Biomaterials 2022;280:121303.
38. Peterson JA, Wijesooriya C, Gehrmann EJ, Mahoney KM, Goswami PP, Albright TR, et al. Family of BODIPY photocages cleaved by single photons of visible/near-infrared light. J Am Chem Soc 2018;140:7343–6.
39. Yang Z, Yifan G, Li P, Weirong K, Kwan M, Weiping W. A green light-enhanced cytosolic protein delivery platform based on BODIPY-protein interactions. Nano Res 2022;16:1042–51.
40. Foster S, Duvall CL, Crownover EF, Hoffman AS, Stayton PS. Intracellular delivery of a protein antigen with an endosomal-releasing polymer enhances CD8 T-cell production and prophylactic vaccine efficacy. Bioconjug Chem 2010;21:2205–12.
41. Kesharwani P, Banerjee S, Gupta U, Mohd Amin MCI, Padhye S, Sarkar FH, et al. PAMAM dendrimers as promising nanocarriers for RNAi therapeutics. Mater Today 2015;18:565–72.
42. Abedi-Gaballu F, Dehghan G, Ghaffari M, Yekta R, Abbaspour-Ravasjani S, Baradaran B, et al. PAMAM dendrimers as efficient drug and gene delivery nanosystems for cancer therapy. Appl Mater Today 2018;12:177–90.
43. Ji Y, Zhao J, Chu C-C. Enhanced MHC-I antigen presentation from the delivery of ovalbumin by light-facilitated biodegradable poly(ester amide)s nanoparticles. J Mater Chem B 2018;6:1930–42.
44. Chefalo PJ, Harding CV. Processing of exogenous antigens for presentation by class I MHC molecules involves post-golgi peptide exchange influenced by peptide-MHC complex stability and acidic pH. J Immunol 2001;167:1274–82.
45. Liu W, Ruan M, Wang Y, Song R, Ji X, Xu J, et al. Light-triggered biomimetic nanoerythrocyte for tumor-targeted lung metastatic combination therapy of malignant melanoma. Small 2018;14:1801754.
46. Alsaab HO, Sau S, Alzhrani R, Tatiparti K, Bhise K, Kashaw SK, et al. PD-1 and PD-L1 checkpoint signaling inhibition for cancer immunotherapy: mechanism, combinations, and clinical outcome. Front Pharmacol 2017;8:561.
47. Carlino MS, Larkin J, Long GV. Immune checkpoint inhibitors in melanoma. Lancet 2021;398:1002–14.
48. Kudo M. Limited impact of anti-PD-1/PD-L1 monotherapy for hepatocellular carcinoma. Liver Cancer 2020;9:629–39.
49. Wu X, Gu Z, Chen Y, Chen B, Chen W, Weng L, et al. Application of PD-1 blockade in cancer immunotherapy. Comput Struct Biotechnol J 2019;17:661–74.
50. Pang L, Ng KT-P, Liu J, Yeung W-HO, Zhu J, Chiu T-LS, et al. Plasmacytoid dendritic cells recruited by HIF-1α/eADO/ADORA1 signaling induce immunosuppression in hepatocellular carcinoma. Cancer Lett 2021;522:80–92.
51. Christian LS, Wang L, Lim B, Deng D, Wu H, Wang X-F, et al. Resident memory T cells in tumor-distant tissues fortify against metastasis formation. Cell Rep 2021;35:109118.
52. Eoli M, Corbetta C, Anghileri E, Di Ianni N, Milani M, Cuccarini V, et al. Expansion of effector and memory T cells is associated with increased survival in recurrent glioblastomas treated with dendritic cell immunotherapy. Neurooncol Adv 2019;1:vdz022.
53. Zhang J, Lyu T, Cao Y, Feng H. Role of TCF-1 in differentiation, exhaustion, and memory of $CD8^+$ T cells: a review. FASEB J 2021;35:e21549.
54. Guan H, Nagarkatti PS, Nagarkatti M. Role of CD44 in the differentiation of Th1 and Th2 cells: CD44-deficiency enhances the development of Th2 effectors in response to sheep RBC and chicken ovalbumin. J Immunol 2009;183:172–80.
55. Duan F, Feng X, Yang X, Sun W, Jin Y, Liu H, et al. A simple and powerful co-delivery system based on pH-responsive metal-organic frameworks for enhanced cancer immunotherapy. Biomaterials 2017;122:23–33.
56. Li AV, Moon JJ, Abraham W, Suh H, Elkhader J, Seidman MA, et al. Generation of effector memory T cell–based mucosal and systemic immunity with pulmonary nanoparticle vaccination. Sci Transl Med 2013;5:204ra130.